Extraction of Robotic Surface Processing Strategies from Human Demonstrations

Thomas Eiband[1], Lars Leimbach[1,2], Korbinian Nottensteiner[1], Alin Albu-Schäffer[1,2]

***Abstract*— Learning from Demonstration (LfD) is a widely used approach for teaching robot motion, but more sophisticated strategies are required to address complex tasks such as surface processing. Sanding is an example where comprehensive strategies are necessary to ensure complete and efficient coverage of the surface of a workpiece. In this paper, we present a system that captures human motions and contact forces during surface processing using a powered sanding tool. We provide a publicly available dataset that consists of demonstrations for various geometric shapes with the goal to extract robot execution strategies through LfD from a variety of users. This is in contrast to conventional LfD, which generates a policy directly from one or multiple trajectories provided by a single user. Further, we provide a data analysis that reveals key insights into how humans adapt their strategies to different surface geometries and extract robot execution strategies from it. Finally, we conduct two basic robotic experiments justifying the approach of strategy extraction. Our findings contribute to the understanding of human surface-processing behavior and lay the foundation for developing more effective robotic surface processing strategies.**

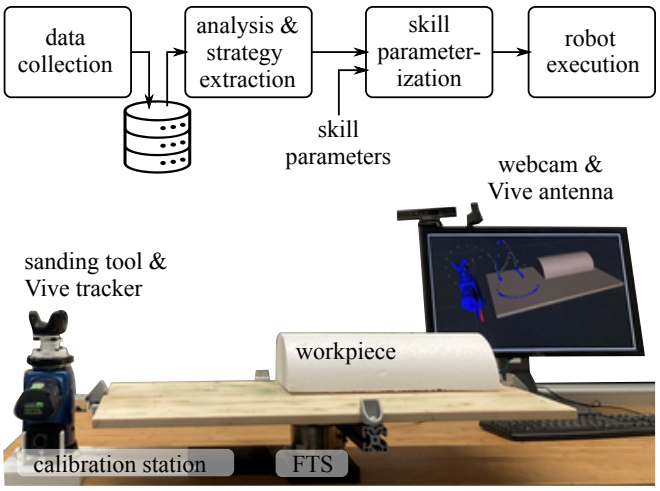

Fig. 1: Data acquisition system for surface processing demonstrations and process from data collection to robot execution.

I. Introduction

Robotic surface processing is a crucial area of research that aims to automate tasks that are often hazardous, monotonous, and physically demanding for humans [1]–[3]. Many surface processing tasks, such as sanding, polishing, or cleaning, are either unsafe or inefficient when performed manually, making them ideal candidates for robotic automation. However, transferring these tasks to robots requires more than mimicking individual human motions — it involves understanding and replicating entire surface processing strategies. While much of the existing work in Learning from Demonstration (LfD) focuses on transferring individual motions from humans to robots [4], [5], our research emphasizes the transfer of comprehensive strategies. These strategies require not only specific motions but also the broader decision-making humans use to adapt to different surfaces and processing conditions.

This work was supported in part by the German Federal Ministry of Education and Research (BMBF) through the "The Future of Value Creation — Research on Production, Services and Work" Program under Grant 02K20D032 and in part by the DLR internal Project "Factory of the Future Extended".

[1]German Aerospace Center (DLR), Institute of Robotics and Mechatronics, Wessling, 82234, Germany

[2]Technical University of Munich, Department of Computer Science, TUM School of Computation, Information and Technology, Munich, 80333, Germany

Corresponding author: thomas.eiband@dlr.de

To this end, we propose a data acquisition system designed to capture and analyze surface processing techniques from a group of human subjects. This system enables us to collect data on how humans handle various surface geometries and processing tasks. Using this data, we extract common patterns and parameters such that robots can reproduce these strategies effectively. Furthermore, there are no data acquisition systems that capture contact force measurements of manually guided, powered sanding tools, which poses a challenge of how a force sensor is embedded into the process.

This work addresses above challenge by a system design that allows contact force sensing while capturing the human tool usage. Since craftsman naturally use their force sensing capabilities to apply the right amount of tool pressure onto the surface, this work publicly provides a dataset consisting of tool motions and forces. In our analysis, the force measurements allowed also to estimate the coverage of the workpiece surface based on the information whether the tool was in contact or not.

Our contributions are 1) the design of a data acquisition system for wireless capturing of human surface processing motions and forces using a powered sanding tool, 2) a data processing pipeline for estimating the tool contact and workpiece coverage, 3) a dataset and an analysis of human surface processing strategies, and 4) the application of an extracted strategy by a real robot.

Through our approach, we have identified several surface

©2025 IEEE. Personal use of this material is permitted. Permission from IEEE must be obtained for all other uses, in any current or future media, including reprinting/republishing this material for advertising or promotional purposes, creating new collective works, for resale or redistribution to servers or lists, or reuse of any copyrighted component of this work in other works. DOI: 10.1109/IROS60139.2025.11247267

processing strategies tailored to various geometries, enabling the development of specialized robotic skills. These skills allow robots to perform surface processing tasks autonomously highlighted in the application at the end of this work.

II. Related Work

Surface processing tasks like sanding [6]–[8], planing [9], or grinding [10] are often executed with powered tools. Commonly used devices are so-called orbital sanders, which often feature a circular finishing disk [6]–[8]. All of these tools execute random or eccentric motions to process the surface in a uniform fashion.

Recording the motion of tools is feasible through commercial tracking systems as presented in [11], [12]. In contrast to motion tracking, force sensing between tool and workpiece is considered more challenging. One approach is to embed the force sensing capability into the tool itself. This can be achieved by integrating a force-torque sensor (FTS) [13]–[17], or by using a mechanical spring, whose deformation together with the tool position change is optically tracked [18]. In all these research works, simplified tools are used that are far from powered sanding tools in real applications. Furthermore, commercially available sanding tools do not have force sensing integrated and adding an FTS would require a challenging redesign of the whole sanding tool. Placing an FTS between the tool handle and the finishing disk is expected to impair the grasp ergonomics and disturb a proper guidance of the tool during the demonstration.

Another approach is to use a robotic system with an additional FTS [7], [8] or a robotic system with integrated force sensing capability [19]. Although, this enables force readings, they can only be measured by using the robotic system during operation. Hand-guiding the robotic system, also known as kinesthetic teaching, is used to program contact based behaviors for surface processing [20], [21]. However, kinesthetic teaching again impedes the human natural strategy due to the robot inertia and kinematic limits. A force sensor can also be integrated into the environment instead of the tool, which is, for instance, used in process monitoring of micro-assemblies [22], to benchmark virtual assemblies [23], or to learn peg-in-hole insertions from human demonstrations [24], which inspired our data acquisition system design.

In summary, demonstration tools exist in different forms and some of them are capable of force sensing. However, there are no known designs for powered sanding tools that also allow force sensing. Furthermore, surface processing tools with force sensing exist that are attached to robotic systems during execution. Using such tools in kinesthetic teaching would allow to record motion and force demonstrations from the human, but would influence the human when dealing with robot inertia and kinematic limits. To overcome all these limitations, we adopt the approach of embedding a force sensor into the environment instead of the tool in our proposed data acquisition system.

III. Data Acquisition System

Our data acquisition system simultaneously captures the motion of the tool through a Vive tracking system and the forces applied through an FTS placed below the workpiece fixture. Figure 2 shows the hardware components and their communication channels. Figure 3 shows the battery-powered sanding tool that was customized based on a commercially available sander of type FESTOOL ETSC 125. Its main modification is an adapter housing with quick-change flange on top for either attaching a damper unit and Vive tracker for motion capturing or attaching the tool to a robot that is later used in the experiments. The damper unit is needed to reduce oscillations on the Vive tracker while the sanding tool is in operation. In the following, we describe the data processing steps.

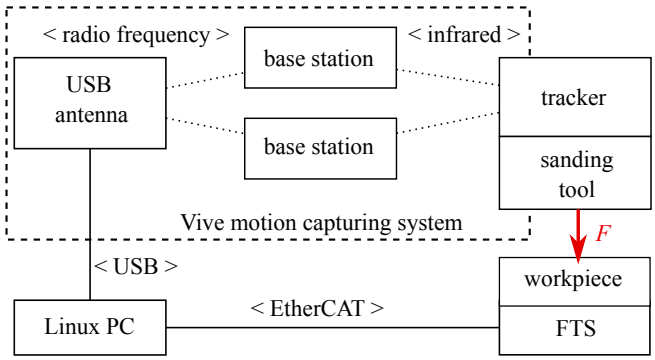

Fig. 2: System components and interfaces (< RF >: radio frequency) with force F applied with the sanding tool by the user.

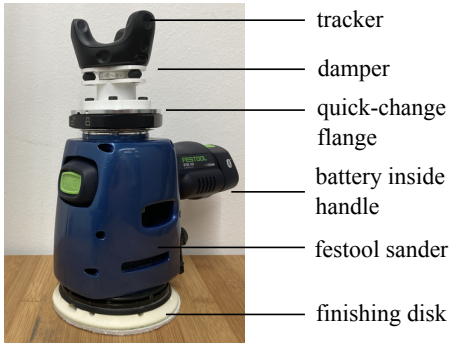

Fig. 3: Powered sanding tool with damper and tracker.

A. Coverage Analysis

The coverage analysis aims to quantify the proportion of the surface that has already been processed. This comes into play when comparing the effectiveness of different user strategies. In this step, we estimate the coverage solely by analysis of the motion and wrench signals of the FTS. Sanding tools usually come with a non-rigid finishing disk (Fig. 3) that can be deformed during operation. Therefore, we need to estimate the tool contact surface rather than a single contact point on the workpiece. We assume that the geometric model of the workpiece is represented as a point

cloud that can be generated from a 3D model file or captured using a stereo or depth camera system. The coverage analysis consists of the following steps: 1) Extraction of contact trajectory; 2) Spawning potential points on finishing disk model; 3) Extraction of closest point set; 4) Density and coverage calculation.

1) Extraction of contact trajectory: In this step, all time steps t of a demonstration trajectory $\boldsymbol{X} = \{\boldsymbol{x}^{(1)}, ..., \boldsymbol{x}^{(T)}\}$ (see Fig. 5a) are identified, for which the absolute force measured by the FTS exceeds a threshold meaning that the tool is in contact with the environment. Removing free motion from the recording leads to a set of contact points denoted as $\boldsymbol{X}_C$ and visualized in Fig. 5b.

2) Spawning potential points on finishing disk model: In this step, we define N points on the circular finishing disk, which are potential contact points. An example with 25 points is shown in (Fig. 4a). For each time step t with

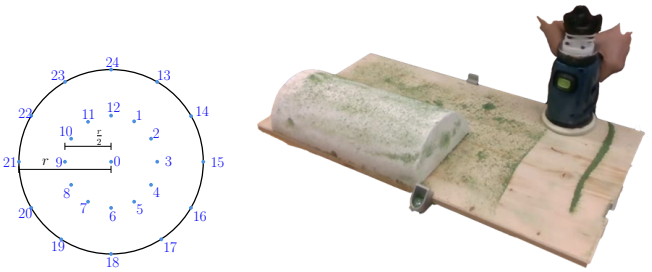

(a) Defined points on finishing disk model with radius r as used in the coverage analysis.

(b) Guide coat serves as feedback for the user during processing and allowed a repeatable data collection process.

Fig. 4

a sample in $\boldsymbol{X}_C$, such set of points is spawned across the finishing disk, denoted as $\boldsymbol{P}_S^{(t)} = \{\boldsymbol{p}_{S,1}^{(t)}, \boldsymbol{p}_{S,2}^{(t)}, \ldots, \boldsymbol{p}_{S,M}^{(t)}\}$. All resulting trajectories are shown in Fig. 5c.

3) Extraction of closest point set: The workpiece point cloud consists of a set of points $\boldsymbol{P}_W = \{\boldsymbol{p}_{W,1}, \boldsymbol{p}_{W,2}, \ldots, \boldsymbol{p}_{W,M}\}$. For any point $\boldsymbol{p}_{W,k}$ in $\boldsymbol{P}_W$ and any point $\boldsymbol{p}_{S,l}^{(t)}$ in $\boldsymbol{P}_S^{(t)}$, we compute their Euclidean distance

$$d_{k,l}^{(t)} = d(\boldsymbol{p}_{W,k}, \boldsymbol{p}_{S,l}^{(t)}) = \|\boldsymbol{p}_{W,k} - \boldsymbol{p}_{S,l}^{(t)}\|\,.$$

By considering all distances below a threshold δ_{contact}, we define the set of points $\boldsymbol{P}_C$ consisting only of points from $\boldsymbol{P}_W$, which can be written as

$$\boldsymbol{P}_C = \{\boldsymbol{p}_{W,k} \in \boldsymbol{P}_W \mid \exists\, \boldsymbol{p}_{S,l}^{(t)} \in \boldsymbol{P}_S^{(t)} \quad \forall \quad k,l,t \text{ such that } d_{k,l}^{(t)} < \delta_{\text{contact}}\}.$$

$\boldsymbol{P}_C$ can be seen as the accumulated set of points on the workpiece that were touched by the sanding tool. Notably, points on the workpiece in $\boldsymbol{P}_W$ may appear multiple times in $\boldsymbol{P}_C$ because the same point in $\boldsymbol{P}_W$ might be the nearest to several other points in $\boldsymbol{P}_S^{(t)}$, which goes into the density calculation in the next step.

4) Density and coverage calculation: We use $\boldsymbol{P}_C$ to compute the spatial density of its individual points. Density estimation can be achieved with various methods, such as with kernel-based or K-nearest neighbors (kNN) methods. We applied kNN as density estimate and compute for each point in $\boldsymbol{P}_C$ the distances between this point and the k neighbors. Figure 5d shows the coverage based on visualizing the density estimate, where the colors in the legend range from blue (low density) to red (high density).

To finally quantify the proportion of the surface that has been already processes, the overall coverage is computed as

$$C = \frac{|\boldsymbol{P}_C'|}{|\boldsymbol{P}_W|},$$

where $|\ldots|$ represents the number of points in $\boldsymbol{P}_C'$ and $\boldsymbol{P}_W$ respectively. Notably, we use a corrected set $\boldsymbol{P}_C'$ that does not contain any duplicate points. This is necessary to keep maximum of the coverage value at 1 referring to 100%, which corresponds to a full coverage of the workpiece surface.

B. Contact Wrench Measurement

Our setup uses an FTS placed under the workpiece. To analyze the forces applied in the contact between the workpiece and tool, we transform the measured wrench to the sanding tool frame by

$${}_C\boldsymbol{W} = \begin{bmatrix} {}_C\boldsymbol{F} \\ {}_C\boldsymbol{M} \end{bmatrix} = \begin{bmatrix} \boldsymbol{R}_{CS} \cdot {}_S\boldsymbol{F} \\ \boldsymbol{R}_{CS} \cdot {}_S\boldsymbol{M} + {}_C\boldsymbol{r}_{CS} \times \boldsymbol{R}_{CS} \cdot {}_S\boldsymbol{F} \end{bmatrix}$$

where ${}_C\boldsymbol{W}$ is the transformed wrench consisting of the force ${}_C\boldsymbol{F}$ and torque ${}_C\boldsymbol{F}$ in the sanding tool frame. ${}_S\boldsymbol{F}$ is the force and ${}_S\boldsymbol{M}$ is the torque in the sensor frame. $\boldsymbol{R}_{\text{CS}}$ is the rotation matrix and ${}_C\boldsymbol{r}_{CS}$ is the translation vector from sanding tool frame $\{C\}$ to FTS frame $\{S\}$ respectively.

IV. Dataset

The surface processing dataset SURP is publicly available[1][2] and contains the tool trajectory, FTS wrench trajectory, and videos from 21 users with varying experience levels in surface processing tasks. Figure 6 shows the different workpieces that were processed, each consisting of one or more multiple basic shapes mounted onto a base plate.

Data was collected following an experimental protocol that instructed the users to process the surface by removing the green guide coat. Full and real surface processing would change the workpiece surface and geometry. Therefore, real surface processing would not have been feasible due to time constraints and the difficulty of repeating the data collection multiple times. The guide coat is a powder that indicates to which extent an area has been already processed by the tool, as shown in Fig. 4b. This step is crucial as it provides the necessary visual feedback to the user about the processing state of the surface. Without a guide coat, users would need

[1]https://doi.org/10.5281/zenodo.16536273
[2]https://teiband.github.io/SURP/

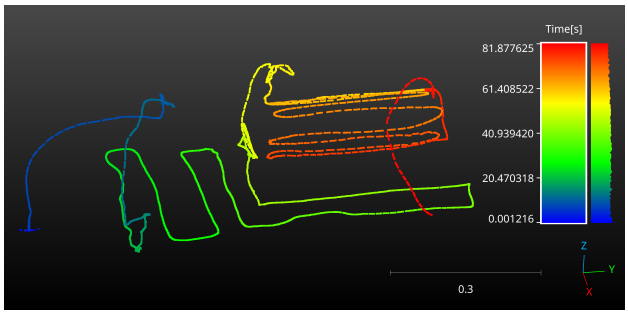

(a) Raw motion trajectory (legend: time axis from blue to red).

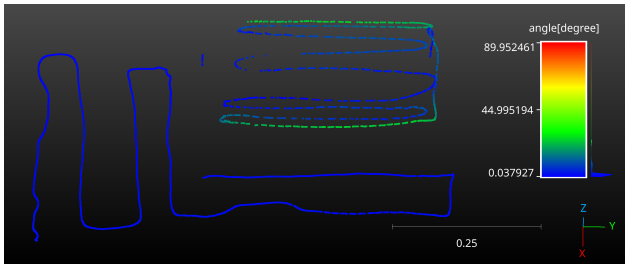

(b) Contact trajectory extracted from motion trajectory (legend: sanding tool angle from blue (0 deg) to red (90 deg).

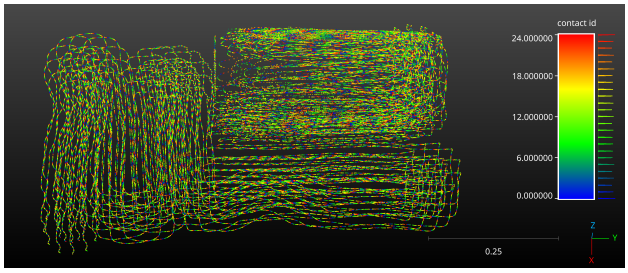

(c) Sampled trajectories for each candidate on the finishing disk (legend: contact id $\in [0, \ldots, 24]$ of potential contact points on finishing disk).

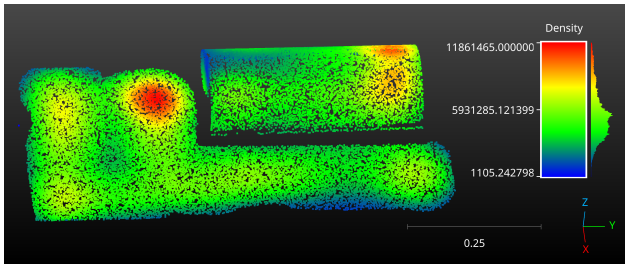

(d) Coverage based on density estimate of contact trajectory (legend: low density (blue), high density (red)).

Fig. 5: Coverage analysis steps for object half-cylinder.

to rely on their mental model about the state of the processed surface area, which could lead to non-optimal coverage due to unprocessed surface patches.

Each of the 21 subjects processed all four workpieces, leading to 84 recorded trajectories. The average age was 26.4 ± 4.5 years. Subjects rated their own experience level on surface processing tasks at an average of 2.33 ± 1.13 on a scale between 1 and 5 with 1 referring to "never" and 5 referring to "once per week". A demonstration on one of the objects took typically between 1.5 to 2 minutes." The tracker sampling rate through the Vive base stations and antenna

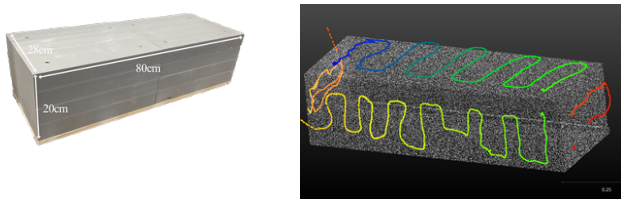

(a) Box

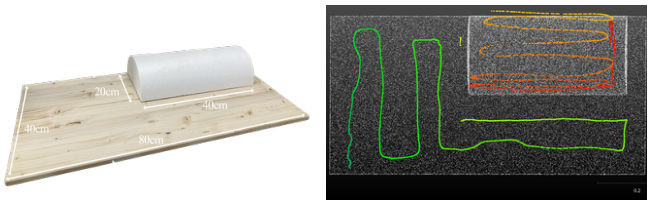

(b) Half-cylinder

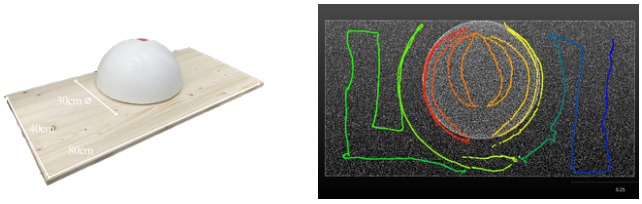

(c) Sphere

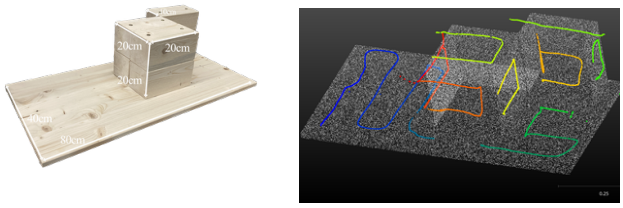

(d) Wooden corners

Fig. 6: Dataset objects with dimensions (left column) and example tool paths from user demonstrations (right column).

reached from 83 to a maximum of 470 Hz with a median rate at 127 Hz. The average speed on the workpiece surface was 0.016 m/s, and the average applied force 47.6 N.

A. *Analysis*

We analyzed the coverage strategies from all users on all workpieces and focused on three factors: the coverage pattern, the usage of micro patterns overlaid onto a global strategy, and the working direction with respect to the geometry. We first focus on the coverage pattern applied to different workpieces. The most frequently used pattern is a snake-like motion. With that, users are going back and forth in parallel lines, which are connected by traverses at each end (see Fig. 6a for an example). Beside the snake pattern, a variety of other patterns could be observed, for instance, as shown for the sphere workpiece in Fig. 7. Figure 8a summarizes which strategy was used per workpiece. It is

evident that users try to minimize the number of lift-offs from the workpiece with the snake pattern. This could be influenced by two factors. First, it reduces physical effort since the sanding tool does not need to be lifted up, and second, it reduces the processing time since the tool always stays in contact with the workpiece.

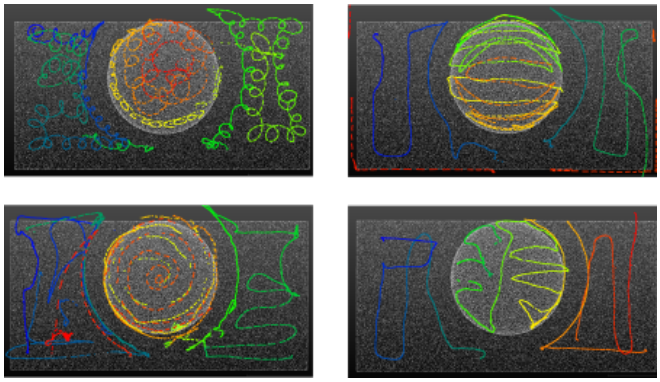

Fig. 7: Different strategies for the sphere workpiece.

Secondly, we test the hypothesis that users move the tool in micro patterns overlaid onto a larger, global strategy. An example can be seen in Fig. 7 (top left), where circular patterns are overlaid onto a global strategy. However, only 22% of all demonstrations contained such kind of strategy. We conclude that this behavior has no advantage over a strategy without micro patterns since it did not increase the coverage value and rather led to increased processing times.

Lastly,we analyze the working direction and how it is aligned with a surface geometry. It is defined as the direction in which the users moved forward during processing to cover an area. For instance, a worker can use a snake pattern to process a part while slowly expanding the covered area from the left to the right, as shown in Fig. 6a. In half of the user trials, the large box was rotated by 90 degree around the z-axis, pointing with either the short or long side to the front of the user. This step assures that the human's ergonomic demands, which might be irrelevant during robotic reproduction, do not influence the choice of the working direction. Regardless of the box orientation, rotated or non-rotated, 81 % of all users selected a working direction along the long side of the rectangular box top surface (Fig. 8b). Although this is not a strategy that minimizes the number of turns when connecting the linear motions, it might have simplified the tracking of the guide coat to estimate the achieved coverage. All coverage values are presented in Fig. 8c showing the highest coverage for the box workpiece. It has the simplest geometry of all workpieces and likely demanded the least complex strategies applied by the subjects.

V. Strategy Reproduction

The goal of this step is to employ a commonly performed user strategy extracted from the dataset to derive a robot skill for efficient reproduction. For a proof of concept, we define skills for two primitive shapes, which are the top plane of the box workpiece and the half-cylinder on the half-cylinder workpiece.

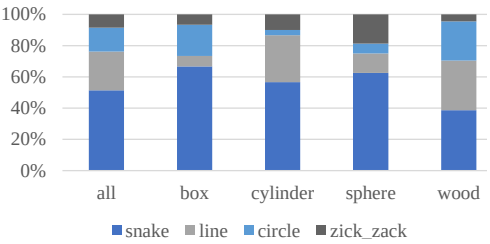

(a) Ratio of observed patterns per object type.

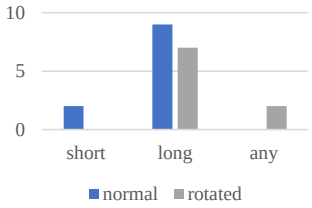

(b) Number of users that selected a working direction along short or long edge of box or any, non-significant direction.

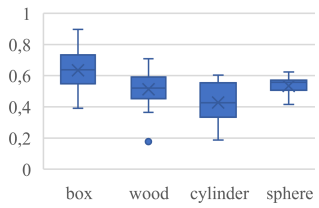

(c) Achieved coverage values of all users per workpiece.

Fig. 8: Statistics on dataset.

A. Plane Skill

- Inputs: `rectangle pose`, `rectangle dimensions`, `tool geometry`
- Outputs: `tool path`, `normal force`

The `rectangle pose` and `rectangle dimensions` allow the plane skill to fit a snake pattern consisting of lines oriented in a main direction connected with turns, hence repeating the pattern in a transverse direction over the surface, as shown in Fig. 9 (left). The main direction aligns with the minor rectangle edge and the transverse direction aligns with the major rectangle edge. The choice of main and transverse directions is taken from the data analysis. The `tool geometry`, circular in our case, governs the pattern repetition frequency and the frame width between tool path and border of the geometrical shape. The `normal force` is computed by the mean normal force of the tool applied onto any side of the box workpiece, which was averaged over all subjects in the dataset, resulting in 42 N. With this skill using the identified strategy from the dataset, a complete coverage could be ensured.

B. Cylinder Skill

- Inputs: `cylinder pose`, `cylinder sector`, `tool geometry`
- Outputs: `tool path`, `normal force`

The `cylinder pose` and `cylinder sector` parameters allow the cylinder skill to fit a snake pattern, similarly as in the planar skill. However, the lines oriented in the

main direction are always aligned with the circumference of the cylinder and the transverse direction is always aligned with the axial direction of the cylinder, no matter what the major and minor dimensions are. This choice is again taken from an analysis of the human strategies in the dataset and ensures that the sanding tool covers a major amount of the cylinder sector. In more detail, the sanding tool processing plate slides over the cylinder circumference, always spanning a contact line in axial direction on the cylinder surface while moving perpendicular to it, hence maximizing the coverage. If the pattern would be oriented perpendicular by 90 degree, the tool would move mainly in axial direction leading to a minimal imprint. With this skill that uses a common strategy from the dataset, almost full coverage of the half-cylinder could be achieved while small patches remained unprocessed. These patches occur on both sides close to the edge between half-cylinder and workpiece base plate and are caused by the radius of the tool finishing disk. The `normal force` is computed by the mean normal force of the tool applied onto the cylinder workpiece, which was averaged over all subjects in the dataset, resulting in $46\,\mathrm{N}$.

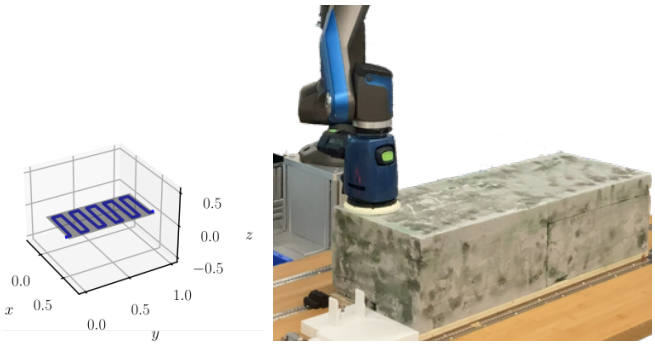

Fig. 9: Processing strategy applied onto a cuboid top surface.

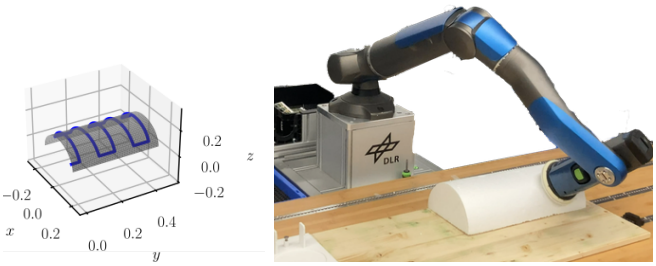

Fig. 10: Processing strategy applied onto a half-cylindrical workpiece.

VI. Discussion

While we were able to acquire a rich set of data from user demonstrations, improvements can be made to the hardware setup. Although different designs for the damper (Fig. 3) between tool and tracker were tested, interruptions in the motion tracking occurred due to occlusions and vibrations caused by the sanding tool, which led to a decrease in the sampling rate. This issues show that developing a low-cost, robust, and portable system requires to solve further challenges in the hardware design.

Therefore, we suggest to evaluate in future work other motion capturing technology, such as optical tracking systems that can work with reflective, passive markers, being less prone to vibrations (e.g. OptiTrack, Vicon). Nevertheless, it is not guaranteed that optical tracking will overcome the problem introduced by vibrations. In theory, using a robot with attached processing tool operated in gravity compensation like in kinesthetic teaching allows a robust motion tracking of the hand-guided tool path. While this approach would overcome the motion tracking problem, it would bias the motion of the human demonstration due to the robot's inertia and kinematic constraints.

Limitations of the presented procedure about extraction of robotic strategies from human demonstrations possibly lie in the human nature of the strategies, which are optimized for anatomical factors and human ergonomics instead of robotic task performance. For example, the most frequently used working direction for the box workpiece was along the long edge. This led to a large number of turns in the snake pattern, which conflicts with an optimal robot strategy that would try to minimize the number of turns on a planar surface. This limitation is not present for the half-cylinder object, which is covered by a human inspired strategy that maximizes the coverage on the cylinder surface. In this case, the main direction of the snake pattern is aligned with the circumference of the cylinder leading to a large tool imprint while moving on the surface. This poses the question, in which scenarios we can best learn valuable strategies from the human, or where a pre-programmed expert strategy is more suitable to account for the robot's technical features.

VII. Conclusion

The proposed system allows for capturing the motions and forces from human subjects providing surface processing demonstrations. The subjects used a powered sanding tool in a natural way without being disturbed by additional cables for sensors. The collected dataset contains the strategies of 21 subjects working on four different environments. Our analysis concluded that the major strategy is a snake-like pattern on planes and cylindrical sectors applied such that it optimizes the coverage from the human perspective.

We use some of the insight gained from the analysis of the presented dataset to apply a meaningful strategy on a real robotic system. With that, we encourage other researchers to learn or extract more dexterous surface processing strategies with the help of our proposed system design and dataset. Furthermore, we would like to investigate more geometric shapes and processing techniques like following edges or smoothing of fine geometric structures. Future work could also consider material properties of real surface finishing tasks with realistic material removal to gain further insights into the strategy of the craftsman.

REFERENCES

[1] F. Nagata, Y. Kusumoto, Y. Fujimoto, and K. Watanabe, "Robotic sanding system for new designed furniture with free-formed surface," *Robotics and Computer-Integrated Manufacturing*, vol. 23, no. 4, pp. 371–379, Aug. 2007.

[2] B. Maric, A. Mutka, and M. Orsag, "Collaborative Human-Robot Framework for Delicate Sanding of Complex Shape Surfaces," *IEEE Robotics and Automation Letters*, vol. 5, no. 2, pp. 2848–2855, Apr. 2020.

[3] J. Nguyen, M. Bailey, I. Carlucho, and C. Barbalata, "Robotic Manipulators Performing Smart Sanding Operation: A Vibration Approach," in *2022 International Conference on Robotics and Automation (ICRA)*, May 2022, pp. 2958–2964.

[4] B. D. Argall, S. Chernova, M. Veloso, and B. Browning, "A survey of robot learning from demonstration," *Robotics and Autonomous Systems*, vol. 57, no. 5, pp. 469–483, 2009.

[5] S. Calinon and D. Lee, "Learning control," in *Humanoid Robotics: a Reference*, P. Vadakkepat and A. Goswami, Eds. Springer, 2018.

[6] S. Schneyer, A. Sachtler, T. Eiband, and K. Nottensteiner, "Segmentation and Coverage Planning of Freeform Geometries for Robotic Surface Finishing," *IEEE Robotics and Automation Letters*, vol. 8, no. 8, pp. 5267–5274, Aug. 2023.

[7] A. Tafuro, C. Ghalloub, A. M. Zanchettin, and P. Rocco, "Autonomous robotic polishing of free-form poly-surfaces:planning from scanning in realistic industrial setting," vol. 232, 2024, pp. 2488–2497.

[8] Y. Wen, D. J. Jaeger, and P. R. Pagilla, "Uniform Coverage Tool Path Generation for Robotic Surface Finishing of Curved Surfaces," *IEEE Robotics and Automation Letters*, vol. 7, no. 2, pp. 4931–4938, Apr. 2022.

[9] A. Montebelli, F. Steinmetz, and V. Kyrki, "On handing down our tools to robots: Single-phase kinesthetic teaching for dynamic in-contact tasks," in *IEEE International Conference on Robotics and Automation (ICRA)*. IEEE, 2015, pp. 5628–5634.

[10] B. Nemec, K. Yasuda, and A. Ude, "A Virtual Mechanism Approach for Exploiting Functional Redundancy in Finishing Operations," *IEEE Transactions on Automation Science and Engineering*, vol. 18, no. 4, pp. 2048–2060, Oct. 2021.

[11] A. M. Eissa, M. R. Atia, and M. R. Roman, "An effective programming by demonstration method for smes' industrial robots," *Journal of Machine Engineering*, vol. 20, 2020.

[12] D. Antonelli and S. Astanin, "Qualification of a collaborative human-robot welding cell," *Procedia CIRP*, vol. 41, pp. 352–357, 2016.

[13] M. Khansari, E. Klingbeil, and O. Khatib, "Adaptive human-inspired compliant contact primitives to perform surface–surface contact under uncertainty," *The International Journal of Robotics Research*, vol. 35, no. 13, pp. 1651–1675, 2016.

[14] W. Meeussen, J. Rutgeerts, K. Gadeyne, H. Bruyninckx, and J. De Schutter, "Contact-state segmentation using particle filters for programming by human demonstration in compliant-motion tasks," *IEEE Transactions on Robotics*, vol. 23, no. 2, pp. 218–231, 2007.

[15] C. V. Perico, J. De Schutter, and E. Aertbeliën, "Learning robust manipulation tasks involving contact using trajectory parameterized probabilistic principal component analysis," in *2020 IEEE/RSJ International Conference on Intelligent Robots and Systems (IROS)*. IEEE, 2020, pp. 8336–8343.

[16] G. Subramani, M. Gleicher, and M. Zinn, "Recognizing geometric constraints in human demonstrations using force and position signals," *IEEE Robotics and Automation Letters*, vol. 3, no. 2, pp. 1252–1259, 2018.

[17] A. Jain, H. Nguyen, M. Rath, J. Okerman, and C. C. Kemp, "The complex structure of simple devices: A survey of trajectories and forces that open doors and drawers," in *2010 3rd IEEE RAS & EMBS International Conference on Biomedical Robotics and Biomechatronics*. IEEE, 2010, pp. 184–190.

[18] Giusti, Zeestraten, Icer, Pereira, Caldwell, Calinon, and Althoff, "Flexible automation driven by demonstration: Leveraging strategies that simplify robotics," *IEEE Robotics & Automation Magazine*, 2018.

[19] M. Iskandar, A. Albu-Schäffer, and A. Dietrich, "Intrinsic sense of touch for intuitive physical human-robot interaction," *Science Robotics*, vol. 9, no. 93, p. eadn4008, Aug. 2024.

[20] T. Eiband and D. Lee, "Identification of common force-based robot skills from the human and robot perspective," in *IEEE-RAS 20th International Conference on Humanoid Robots (Humanoids)*. IEEE, 2021, pp. 507–513.

[21] T. Eiband, J. Liebl, C. Willibald, and D. Lee, "Online task segmentation by merging symbolic and data-driven skill recognition during kinesthetic teaching," *Robotics and Autonomous Systems*, vol. 162, p. 104367, 2023.

[22] S. Tangjitsitcharoen, P. Tangpornprasert, C. Virulsri, and N. Rojanarowan, "In-process monitoring and control of microassembly by utilising force sensor," *Journal of Achievements in Materials and Manufacturing Engineering*, no. Vol. 31, nr 2, pp. 588–594, 2008.

[23] M. Sagardia and T. Hulin, "Multimodal Evaluation of the Differences between Real and Virtual Assemblies," *IEEE Transactions on Haptics*, vol. 11, no. 1, pp. 107–118, Jan. 2018.

[24] K. Wang, Y. Zhao, and I. Sakuma, "Learning Robotic Insertion Tasks From Human Demonstration," *IEEE Robotics and Automation Letters*, vol. 8, no. 9, pp. 5815–5822, Sep. 2023.